Deformation energy of a toroidal nucleus and plane fragmentation barriers

C. Fauchard, Guy Royer, E. Druet

SUBATECH
Laboratoire de Physique Subatomique
et des Technologies Associées
UMR Université - EMN - IN2P3 / CNRS

DEFORMATION ENERGY OF A TOROIDAL NUCLEUS AND PLANE FRAGMENTATION BARRIERS

C.Fauchard, G. Royer and E. Druet

Rapport Interne SUBATECH -95-10

DEFORMATION ENERGY OF A TOROIDAL NUCLEUS AND PLANE FRAGMENTATION BARRIERS

C.Fauchard, G.Royer et E.Druet

Laboratoire de physique subatomique et des technologies associées
UMR : IN2P3/CNRS, Université et Ecole des Mines de Nantes
4 rue A.Kastler, La Chantrerie - 44070 - Nantes-Cedex 03 - France

Abstract : The path leading to pumpkin-like configurations and toroidal shapes is investigated using a one-parameter shape sequence. The deformation energy is determined within the analytical expressions obtained for the various shape-dependent functions and the generalized rotating liquid drop model taking into account the proximity energy and the temperature. With increasing mass and angular momentum, a potential well appears in the toroidal shape path. For the heaviest systems, the pocket is large and locally favourable with respect to the plane fragmentation barriers which might allow the formation of evanescent toroidal systems which would rapidly decay in several fragments to minimize the surface tension.

1.Introduction

Heavy-ion accelerators delivering projectile energy up to 100 MeV/u and very efficient 4π detectors [1-2] are now available and, besides the fusion, fission, evaporation and deep-inelastic regime, the nuclear fragmentation corresponding to the emission of several intermediate mass fragments and the vaporization related to the decay into many light particles can now be obtained [3-5]. The underlying physics responsible for the fragmentation process is still debated [6] and the possibilities of the simultaneous explosion of a very hot system and of the sequential breakup of excited fragments have been advanced. Experimentally, the two scenarii seem possible since, for example, analyses of the data (within the cascade fission approach) have shown that the average time between two successive binary decays decreases from more than 500 fm/c to less than 50 fm/c when the beam energy increases from 30 to 60 MeV/u in the Ar + Au reaction [7]. From branching ratios for different decay channels it has also been asserted [8] that the sources decay in a statistical manner. Nevertheless, the role of the dynamics in the entrance channel is essential since a considerable portion of the mass, energy and angular momentum is radiated before the decay causing a significant reduction of the fragmentation width [9].

The successful statistical fragmentation models [10-11] presently employ sources with uniform interiors. It is questionable whether the dynamics in such violent collisions lead really to homogeneous quasi-spherical nuclear systems or whether the compression and expansion effects induce spinodal, surface or Coulomb instabilities [12]. Recently, exotic nuclear shapes like tori and bubbles were observed in simulations within microscopic transport models [13-18]. These topologies were early suggested as being metastable long time ago [19-20]. A number of observables have been proposed which might signal the decay of toroidal configurations [13,14,16,17] but the formation of tori has not yet been experimentally confirmed though it seems that several intermediate mass fragments emitted almost in the same plane have been observed [21]. To have a first rough estimate of these exotic exit channels, the fragmentation barriers into several spherical nuclei in a volume-like manner [22] and in a ring-like manner [23] have been recently determined and compared within the liquid drop model including the nuclear proximity energy and the finite temperature. The 3, 4, 6 and 8 nascent fragments were spatially symmetrically arranged ; the geometric configurations being respectively equilateral triangle, tetrahedron, spheres along three Cartesian axes and cube in the first case and equilateral triangle, square, hexagon and octogon for the two-dimensional emission. It was found that the plane fragmentation barriers are always lower than the ones corresponding to the emission in the whole space.

In the present work we determine the energy of a nucleus in the deformation path leading continuously from the initial spherical shape towards toroidal configurations and compare with the plane fragmentation barriers. The purpose is to know to what extent evanescent toroidal nuclear systems might survive before decaying into several fragments. In sect.2 the selected one-dimensional shape sequence starting from the sphere and roughly reproducing the first steps of the toroidal deformation valley is defined. Analytical expressions are given for the different geometric characteristics such as volume, moment of inertia, root-mean-square radius,.. in sect.3. In sect.4 the surface and Coulomb shape-dependent functions are calculated. The dependence of the toroidal deformation barriers on the mass, temperature and rotation is displayed in sect.5. Finally, the barriers standing in the different exit channels are compared in sect.6.

2. Oblate elliptic lemniscatoid and torus

The family of elliptic lemniscates allows to describe continuously the transition from one circle to two-tangent circles [24]. In polar coordinates in the (x,z) plane the lemniscate is defined by (see figure 1) :

$$R^2(\theta) = a^2 \cos^2\theta + c^2 \sin^2\theta \tag{2.1}$$

where a and c are the semi-axis lengths. In cartesian coordinates the equation reads :

$$c^2x^2 + a^2z^2 = (x^2 + z^2)^2. \tag{2.2}$$

The solid (called later oblate elliptic lemniscatoids) generated by the rotation around the z axis has a pumpkin-like configuration. Assuming volume conservation, the unique dimensionless parameter s = a/c is sufficient to define the shape completely. When s decreases from 1 to 0, an hollow progressively appears and the oblate lemniscatoid varies continuously from a sphere to a torus for which the upper and lower hollows are just linked. Later on, the evolution from this initial toroidal shape towards torii with large radius r_t can be governed by :

$$s = (r_t - r_s)/2r_s \qquad 0 \le s \le s_{max} \tag{2.3}$$

where s_{max} corresponds to a realistic limit of the sausage radius r_S.
The following parameters are also of interest :

$$\begin{aligned} a &= r_t - r_s \\ b &= r_t + r_s \\ c &= b - a = 2r_s . \end{aligned} \tag{2.4}$$

3. Geometric characteristics

As for the prolate elliptic lemniscatoids (obtained by a rotation around the x axis) used in fission and fusion studies [24,25] we obtain analytical expressions for the various shape-dependent functions. The volume, relative perpendicular moment of inertia and the relative mean square radius of the oblate elliptic lemniscatoids are given by :

$$V = \frac{4\pi R_0^3}{3} = \frac{4\pi c^3}{3}\left(\frac{s^3}{4} + \frac{3s}{8} + \frac{3}{8}\frac{\sin^{-1}\sqrt{1-s^2}}{\sqrt{1-s^2}}\right) \tag{3.1}$$

$$I_{\perp rel} = \frac{I_\perp}{\frac{2}{5}mR_0^2} = \frac{3c^5}{2R_0^5(1-s^2)}\left(-\frac{s^7}{24} - \frac{s^5}{16} - \frac{25s^3}{192} + \frac{35s}{128} - \frac{5}{16}\left(s^2 - \frac{7}{8}\right)\frac{\sin^{-1}\sqrt{1-s^2}}{\sqrt{1-s^2}}\right) \tag{3.2}$$

$$\langle r^2 \rangle_{rel} = \frac{\langle r^2 \rangle}{\frac{3}{5}R_0^2} = \frac{5c^5}{4R_0^5}\left(\frac{2s^5}{15} + \frac{s^3}{6} + \frac{s}{4} + \frac{1}{4}\frac{\sin^{-1}\sqrt{1-s^2}}{\sqrt{1-s^2}}\right) \tag{3.3}$$

where R_0 is the radius of the initial sphere.

For an holed torus, the same quantities are defined by :

$$V = \frac{4\pi R_0^3}{3} = 2\pi^2 r_t r_s^2 = \frac{\pi^2 c^3}{4}(1+2s) \tag{3.4}$$

$$I_{\perp rel} = \frac{35}{32}(1 + 3s + 3s^2)\left(\frac{16}{3\pi(1+2s)}\right)^{2/3} \tag{3.5}$$

$$< r^2 >_{rel} = \frac{5}{6}(1 + 2s + 2s^2)\left(\frac{16}{3\pi(1+2s)}\right)^{2/3}. \tag{3.6}$$

From (3.4) it follows :

$$r_s = R_0(\frac{2}{3\pi(1+2s)})^{1/3} \tag{3.7}$$

As an illustration, for s = 0, 1, 2 and 3 one obtains respectively $<r^2>^{1/2}$ = 1.089, 1.688, 2.296 and 2.846, r_s/R_0= 0.596, 0.414, 0.349 and 0.312 and r_t/r_S =1, 3, 5 and 7.

In figures 2 and 3 the variations of s and $I_{\perp rel}$ versus the relative r.m.s radius are displayed and compared with the values in the new binary fission valley corresponding to compact and creviced shapes rapidly leading to two spherical fragments and approximated by prolate lemniscatoids and two separated spheres. For a same s ratio, the r.m.s radius is greater in the binary fission path since the matter distribution is farther from the centre. The moment of inertia varies very smoothly when the nuclear shape evolves from the sphere to oblate lemniscatoids and later to large torii and the curve profiles are identical in the two deformation valleys.

4. Relative surface and Coulomb energies

The relative surface energy can be expressed as :

$$B_s = \frac{s}{4\pi R_0^2} = \frac{c^2}{2R_0^2}(s^2 + \frac{\sin^{-1}\sqrt{1-s^4}}{\sqrt{1-s^4}}) \tag{4.1}$$

for the pumpkin-like configurations and as :

$$B_s = \frac{4\pi^2 r_t r_s}{4\pi R_0^2} = \frac{\pi c^2}{4R_0^2}(1+2s) \tag{4.2}$$

for the torus.

For the non-holed shape, the relative Coulomb energy has been evaluated using the method of Cohen and Swiatecki [26]

$$B_c = 1/2 \cdot \int \frac{v(\theta_i)}{v_0}\left(\frac{R(\theta_i)}{R_0}\right)^3 \sin\theta_i d\theta_i \tag{4.3}$$

where the electrostatic potential $v(\theta_i)$ is calculated at the surface of the shape and v_0 is the surface potential of the sphere.

$$\frac{v(\theta_i)}{v_0} = \frac{3}{4\pi R_0^2} \cdot 2 \cdot \int \frac{A(\theta,\theta_i)K(k) - k^2 B(\theta,\theta_i)D(k)}{C(\theta,\theta_i)} d\theta \tag{4.4}$$

with

$$A(\theta,\theta_i) = R(\theta)\sin\theta[R(\theta)R(\theta_i)\cos(\theta+\theta_i) + c^2(1-s^2)\frac{R(\theta_i)}{R(\theta)}\cos\theta\sin\theta\sin(\theta+\theta_i) - R^2(\theta)]$$

$$B(\theta,\theta_i) = [R^2(\theta_i) + R^2(\theta) - 2R(\theta_i)R(\theta)\cos(\theta+\theta_i)] \cdot [-R(\theta)\sin\theta + c^2(1-s^2)\frac{\sin\theta\cos^2\theta}{R(\theta)}] \tag{4.5}$$

$$C(\theta,\theta_i) = [R^2(\theta_i) + R^2(\theta) - 2R(\theta_i)R(\theta)\cos(\theta+\theta_i)]^{1/2}$$

and

$$D(k) = \frac{K(k) - E(k)}{k^2}. \tag{4.6}$$

E and K are the complete elliptic integrals of the argument k given by :

$$k^2 = \frac{4R(\theta)R(\theta_i)\sin\theta\sin\theta_i}{R^2(\theta_i) + R^2(\theta) - R(\theta_i)R(\theta)\cos(\theta+\theta_i)} \tag{4.7}$$

For the toroidal configurations the shape-dependent Coulomb function has been calculated within the method of Wong [27]

$$B_c = \frac{5}{6}\left(\frac{3\pi}{2\cosh^2\eta_0}\right)^{1/3} \frac{\sinh^5\eta_0}{\cosh\eta_0}\left[\frac{8}{9\pi^3}\sum_{n=0}^{\infty}\varepsilon_n B_n(\cosh\eta_0)C_n(\cosh\eta_0) - \frac{\cosh\eta_0}{8\pi\sinh^5\eta_0}(4\cosh^2\eta_0 + 3)\right]$$

(4.8)

where the toroidal coordinate η_0 and the r_t and r_s radii are connected with :

$$\eta_0=\cosh^{-1}(r_t/r_s) \tag{4.9}$$

$$r_t=R_0(2\cosh^2\eta_0/3\pi)^{1/3} \tag{4.10}$$

$$r_s=R_0(2/(3\pi\cosh\eta_0))^{1/3} \tag{4.11}$$

and

$$\begin{aligned} B_n(x) &= (n+1/2)P_{n+1/2}(x)Q^2_{n-1/2}(x)-(n-3/2)P_{n-1/2}(x)Q^2_{n+1/2}(x) \\ C_n(x) &= (n+1/2)Q_{n+1/2}(x)Q^2_{n-1/2}(x)-(n-3/2)Q_{n-1/2}(x)Q^2_{n+1/2}(x) \\ \varepsilon_n &= 2-\delta_{n0}, \end{aligned} \tag{4.12}$$

P and Q are the Legendre functions of first and second kind.

The general trends of the B_s and B_c shape-dependent functions are displayed in figure 4. The matter moves essentially on a plane for the pumpkin-like configurations and torii while it changes place on an axis in the case of the fission and, consequently, for a given r.m.s radius the B_s and B_c functions have respectively more increased and decreased in the toroidal shape valley. In the binary decay path and, more generally, in the path leading to n spherical fragments, the surface is constant once the rupture of the bridge of matter between the nascent fragments is realized. In contrast, the surface energy increases infinitely with the torus radius which is the main explanation of the instability of this topology.

5. L and T dependent toroidal deformation barriers

Assuming volume conservation and within the generalized liquid drop model including the nuclear proximity effects and the temperature, the energy of a rotating deformed nucleus relatively to the energy of the non-rotating sphere may be defined as [22-25]

$$E_{def}=\frac{3e^2Z^2}{5R_0}(B_c-1)+a_s(1-2.6I^2)A^{2/3}(B_s-1)+E_{prox}+\frac{\hbar^2l(l+1)}{2I_\perp} \tag{5.1}$$

with I=(N-Z)/A. The proximity term supplements the surface energy to take into account the attraction between the surfaces in regard in the hollows of the oblate lemniscatoids and in the hole of the torus.

The temperature dependences of the surface coefficient and the effective sharp radius are defined as :

$$a_S=17.9439(1+1.5T/17)(1-T/17)^{3/2}\ \text{MeV} \tag{5.2}$$

$$R_0=(1.28A^{1/3}-0.76+0.8A^{-1/3})(1+0.0007T^2)\ \text{fm}. \tag{5.3}$$

Such a prescription leads to the L and T dependent barriers displayed in figures 5, 6 and 7 for ^{147}Tb, ^{240}Pu and ^{322}128. In the whole isotope table, a high barrier stands in the toroidal deformation path at T = 0 preventing the non-rotating nuclei to investigate the torus shape. For the heaviest nuclear systems of mass around 300-350 accessible as residue after evaporation in heavy-ion reactions at intermediate energies (such as Gd+U, Au+Au, Pb+Au) the potential barriers present two wells. The first one is located closely to the shape at s = 0 while the second one is very large the minimum of which corresponding roughly to a relative r.m.s radius of 1.85 and $r_t \sim 2.3\ r_S$. With increasing angular momenta, the two deformed minima appear in the whole mass range. The first one disappears progressively at the highest angular momenta while the outer one is pushed to very large deformations. The potential energy is lowered by the temperature. For example at T= 6 MeV and for ^{240}Pu a deformed minimum appears already at l = 0. For the heaviest masses, only the first inner minimum remains and disappears relatively rapidly with increasing angular momenta.

6. Comparison between the toroidal shape path and the plane fragmentation

In figures 8, 9 and 10 the deformation energy in the toroidal shape path is compared with the plane fragmentation barriers encountered by n equal fragments symmetrically arranged on regular polygon configurations. In the case of the planar fragment emission, the barrier tops always correspond to separated fragments maintained in unstable equilibrium by the balance between the repulsive Coulomb forces and the attractive nuclear forces. The barrier heights increase with the number of fragments except for the hot heaviest systems. For masses below around 220 the absence of potential energy minimum for the non-rotating toroidal configurations, even at high temperature, seems to forbid the smallest stability. Furthermore, the deformation energy is greater than the one of the polygon configurations. For the heaviest existing systems, the situation is reverse since a wide and deep potential pocket appears and is lower than the potential barriers for the n fragment emission in some deformation range. This might perhaps allow to such exotic toroidal shapes, generated by the dynamics in the first phase of the most massive heavy-ion collisions, to survive in a metastable state before decaying in the multifragment exit channels due to the effects of the surface tension forces which clusterize the matter distribution to minimize the nuclear surface. The angular momentum transfer accompanying the formation of these toroidal shapes in heavy-ion reactions might also slightly increase their stability.

7. Conclusion

The path leading to rotating pumpkin-like configurations and toroidal shapes at finite temperature has been investigated using a one-parameter shape sequence and within the generalized liquid drop model taking into account the proximity energy. The geometric characteristics such as root-mean-square radius, volume, surface and moment of inertia are given analytically.

At T = 0, a high regular barrier without deformed minimum stands for all nuclear masses preventing the non-rotating nuclei to investigate the toroidal shapes. For the heaviest nuclear systems, accessible as residue in heavy-ion reactions, a deep and wide potential pocket appears corresponding to torus with a large hole. With increasing angular momentum and temperature the potential barriers present two minima in the whole mass range. The shape of the inner minimum is a torus with a nascent hole, it disappears at the highest angular momenta. For masses higher than about 200 the potential energy is lower in the toroidal deformation path than in the n fragment decay paths for some deformation range increasing with the mass. If the dynamics in the most massive heavy-ion collisions leads the system in the toroidal configuration valley, the presence of a well in the deformation barrier ,which is moreover locally lower than the plane fragmentation barriers, might allow to these exotic toroidal shapes to survive in a metastable state before decaying into n fragments to minimize the surface tension.

REFERENCES

1) J. Galin and U. Jahnke, J. of Phys. **G20** (1994) 1105
2) F. Saint-Laurent, Nucl. Phys. **A 583** (1995) 481c
3) J.F. Lecolley et al, Phys. Lett. **B325** (1994) 317
4) W.G. Lynch, Nucl. Phys. **A583** (1995) 471c
5) C.O. Bacri et al, preprint CEA/DAPNIA/SPhN 57 (1994)
6) A.S. Botvina and D.H.E. Gross, Phys. Lett. **B344** (1995) 6
7) M. Louvel et al, Phys. Lett. **B320** (1994) 221
8) L.G. Moretto, D.N. Delis and G.J. Wozniak, Phys. Rev. Lett **71** (1993) 3935
9) J.A. Lopez and J. Randrup, Nucl. Phys. **A 571** (1994) 379
10) J.P. Bondorf, R. Donangelo, I.N. Mishustin, C.J. Pethick, H. Schutz and K. Sneppen, Nucl. Phys. **A443** (1985) 231
11) D.H.E Gross, Rep. Prog. Phys. **53** (1990) 605
12) L.G. Moretto, K. Tso and G.J. Wozniak, preprint LBL 34724-UC413 (1993)
13) L.G. Moretto, K. Tso, N. Colonna and G.J. Wozniak, Phys. Rev. Lett. **69** (1992) 1884
14) W. Bauer, G.F. Bertsch and H.Schulz, Phys. Rev. Lett. **69** (1992) 1888
15) S.R. Souza and C.Ngô, Phys. Rev. **C48** (1993) R2555
16) H.M. Xu, C.A. Gagliardi, R.E. Tribble and C.Y. Wong, Phys. Rev. **C49** (1994) R1778 and Nucl. Phys. **A 569** (1994) 575
17) D.O. Handzy, S.J. Gaff, W. Bauer, F.C. Daffin, C.K. Gelbke and G.J. Kunde, Phys. Rev. **C51** (1995) 2237
18) B.Jouault, F.Sebille, G.Royer and V. de la Mota, Nucl. Phys. **A** (1995) in press
19) J.A. Wheeler, Nucleonics notebook (1950) unpublished
20) P. Siemens and H. Bethe, Phys. Rev. Lett. **18** (1967) 704
21) D. Durand, Ganil symposium " Advances in nuclear physics ", Le Pradet, France, (1995)
22) F. Haddad and G. Royer, J.of Phys. **G18** (1992) L153
23) G. Royer and F. Haddad, J. of Phys. **G20** (1994) L131
24) G. Royer and B. Remaud, J. of Phys. **G10** (1984) 1057
25) G. Royer and B. Remaud, Nucl. Phys. **A444** (1985) 477
26) S. Cohen and W.J. Swiatecki, Ann. of Phys. **22** (1963) 406
27) C.Y. Wong, Ann. of Phys. **77** (1973) 279

FIGURE CAPTIONS

Figure 1 : Oblate elliptic lemniscatoids as a function of the ratio s of the minor a and major c semi-axes and torus defined by the sausage r_s and torus r_t radii. Oz is the axis of revolution. Volume conservation is assumed.

Figure 2 : Variation of s as a function of the relative root-mean-square radius. The full curve corresponds to the oblate lemniscatoid and toroidal shapes and the dashed curve to the prolate lemniscatoid and two sphere shapes (new fission valley).

Figure 3 : Relative perpendicular moment of inertia as a function of the relative root-mean-square radius. The full curve corresponds to the oblate lemniscatoid and toroidal shapes and the dashed curve to the prolate lemniscatoid and two sphere shapes.

Figure 4 : Variation of the surface B_S and Coulomb B_C shape-dependent functions as a function of the relative root-mean-square radius. The full curve is relative to the oblate lemniscatoid and toroidal shapes and the dashed curve to the prolate lemniscatoid and two sphere shapes. The vertical dashed and dotted curve corresponds to the transient case s = 0.

Figure 5 : Sum of the deformation and rotational energies at T = 0 and 6 MeV as functions of the r.m.s radius and angular momentum for ^{147}Tb in the toroidal shape path.

Figure 6 : Same as figure 5 but for ^{240}Pu.

Figure 7 : Same as figure 5 but for ^{322}128.

Figure 8 : Comparison at T = 0 and T = 6 MeV between the toroidal deformation barrier (full curve) and barriers of plane fragmentation into 2, 3, 4, 6 and 8 fragments (dashed curves) for ^{147}Tb.

Figure 9 : Same as figure 8 but for ^{240}Pu.

Figure 10 : Same as figure 8 but for ^{322}128.

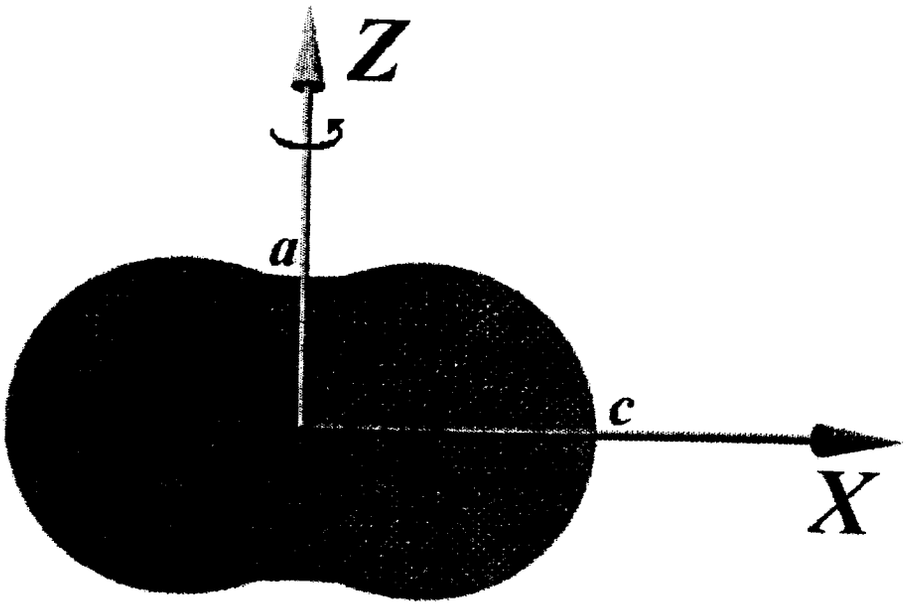

$S = 0.50$

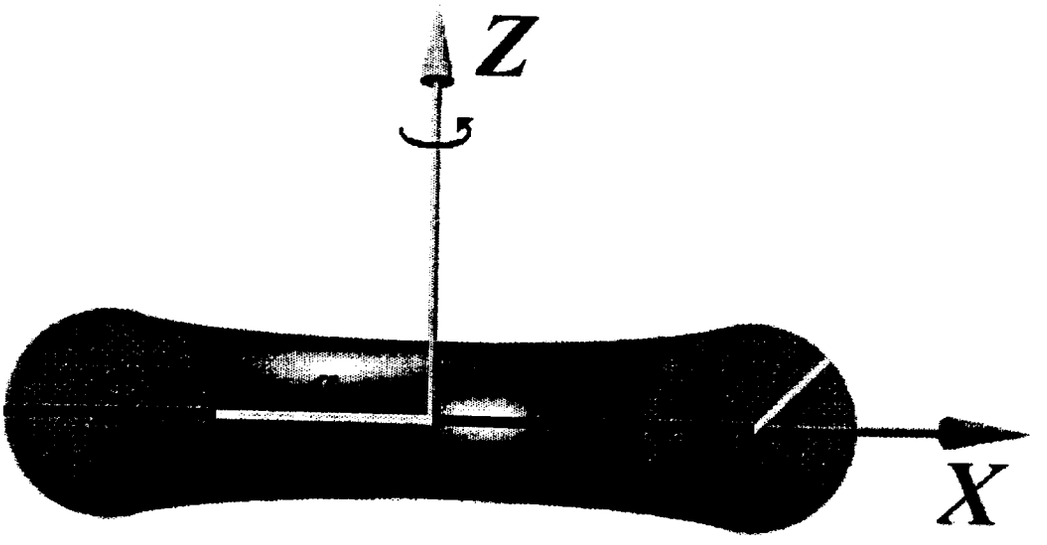

$S = 1.00$

Figure 1a

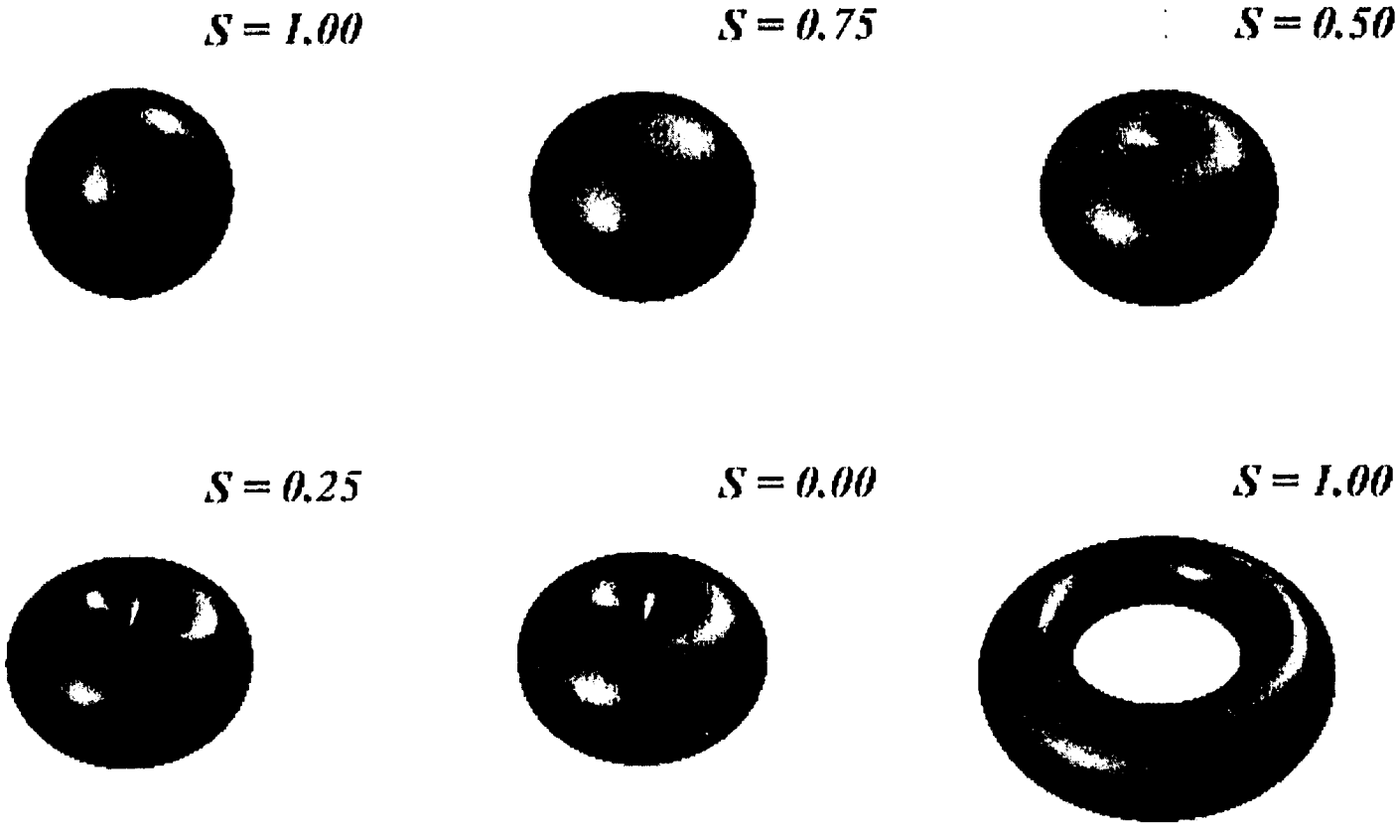

Figure 1b

Figure 2

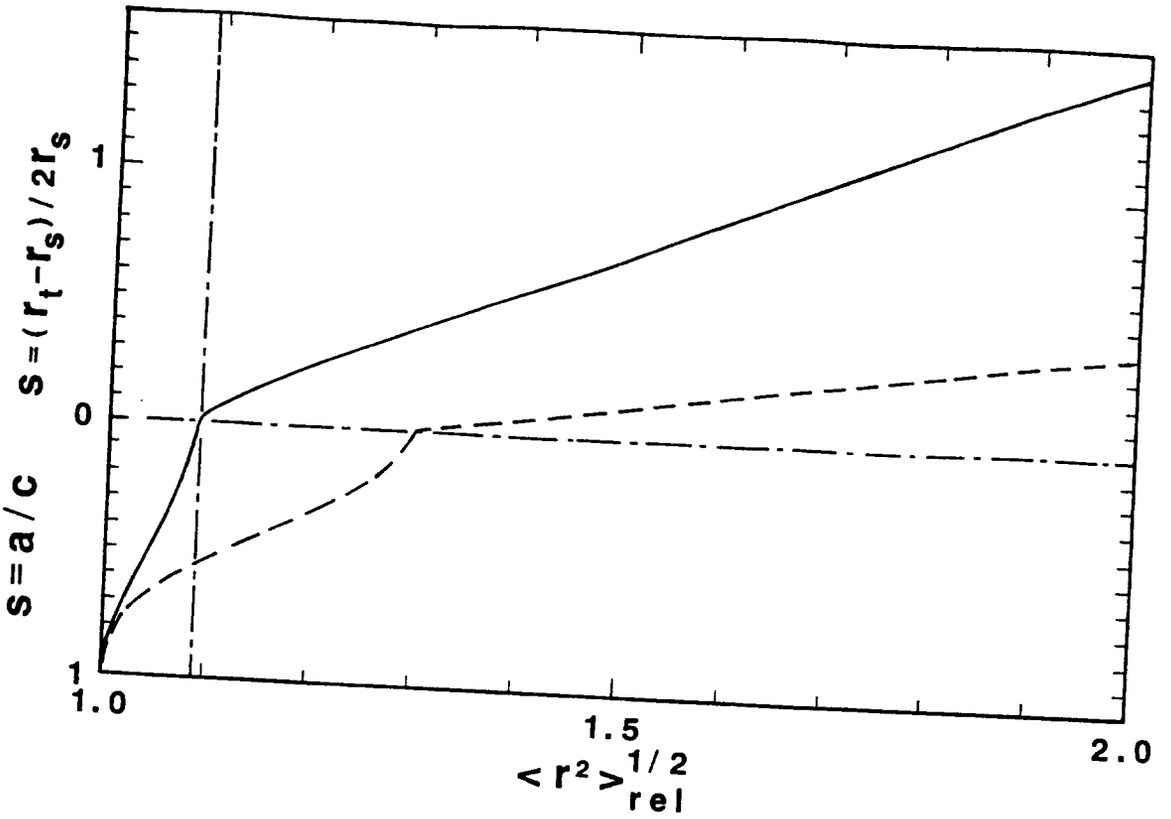

Figure 3

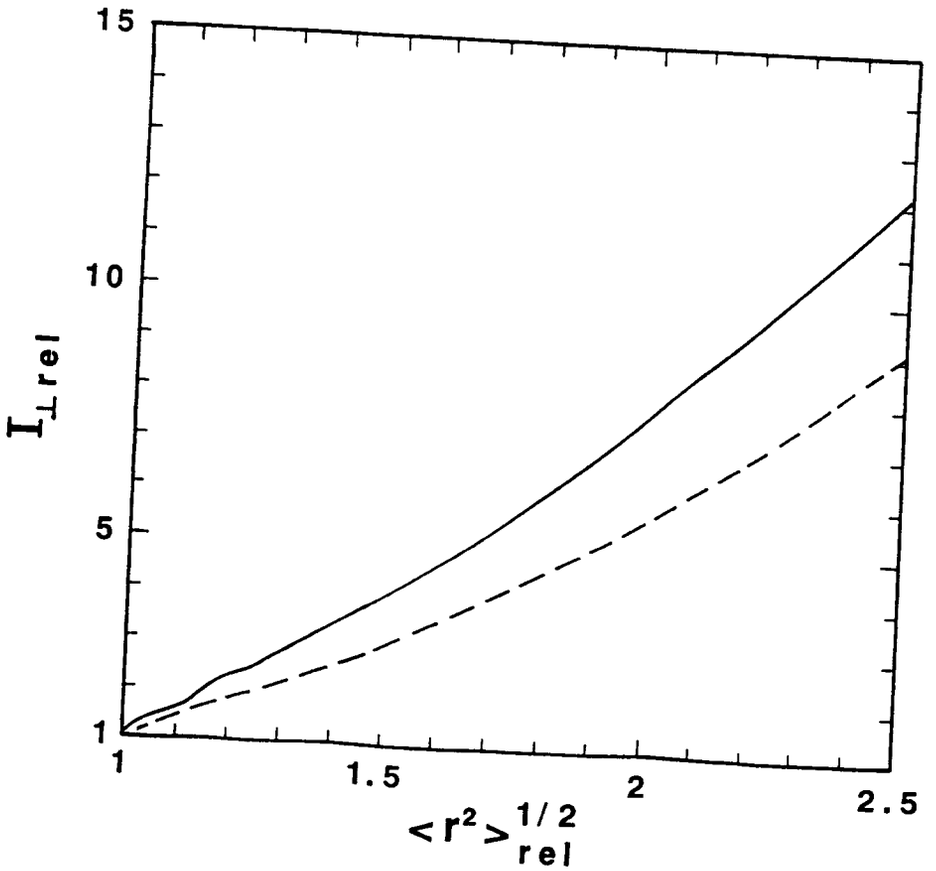

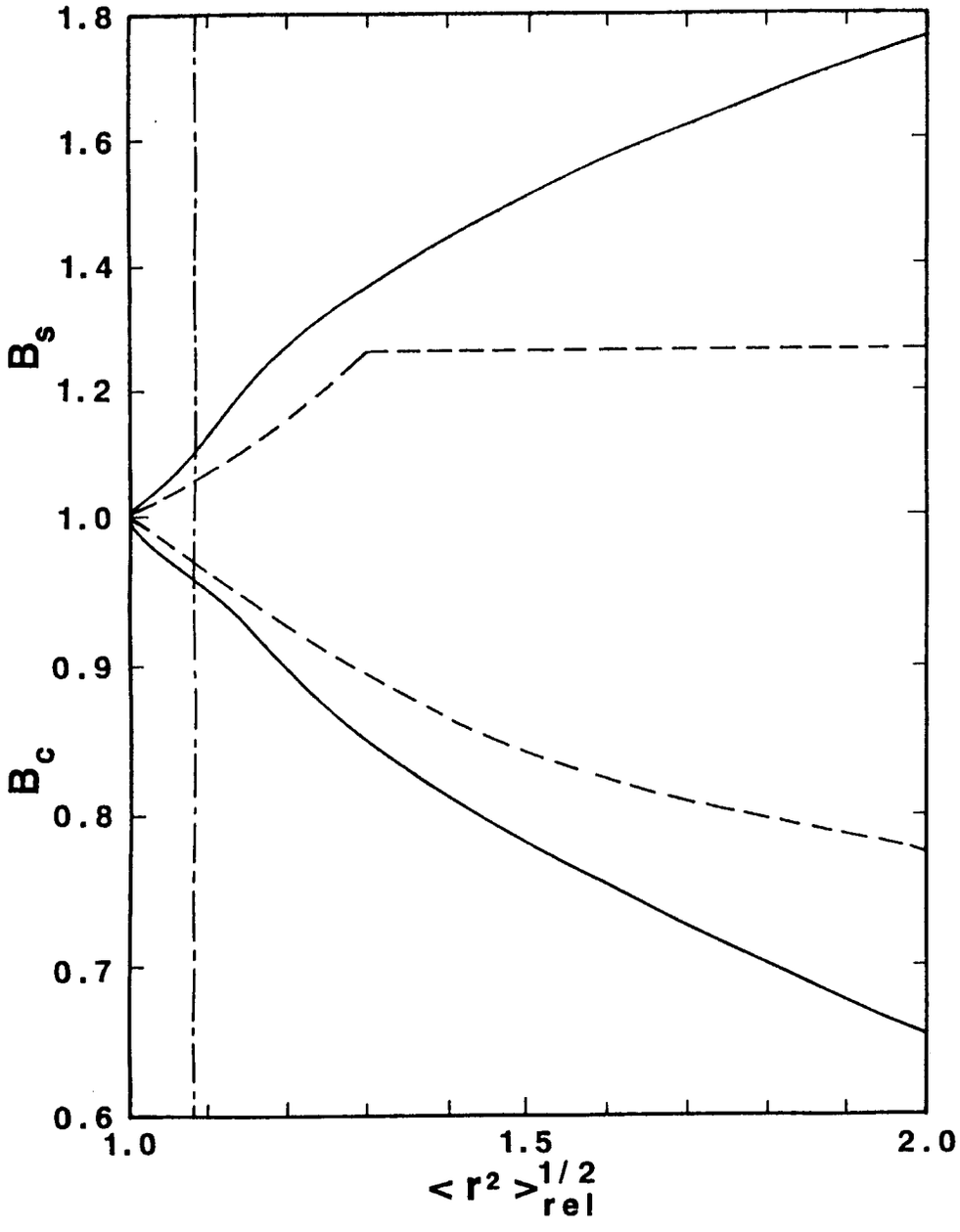

Figure 4

Figure 5

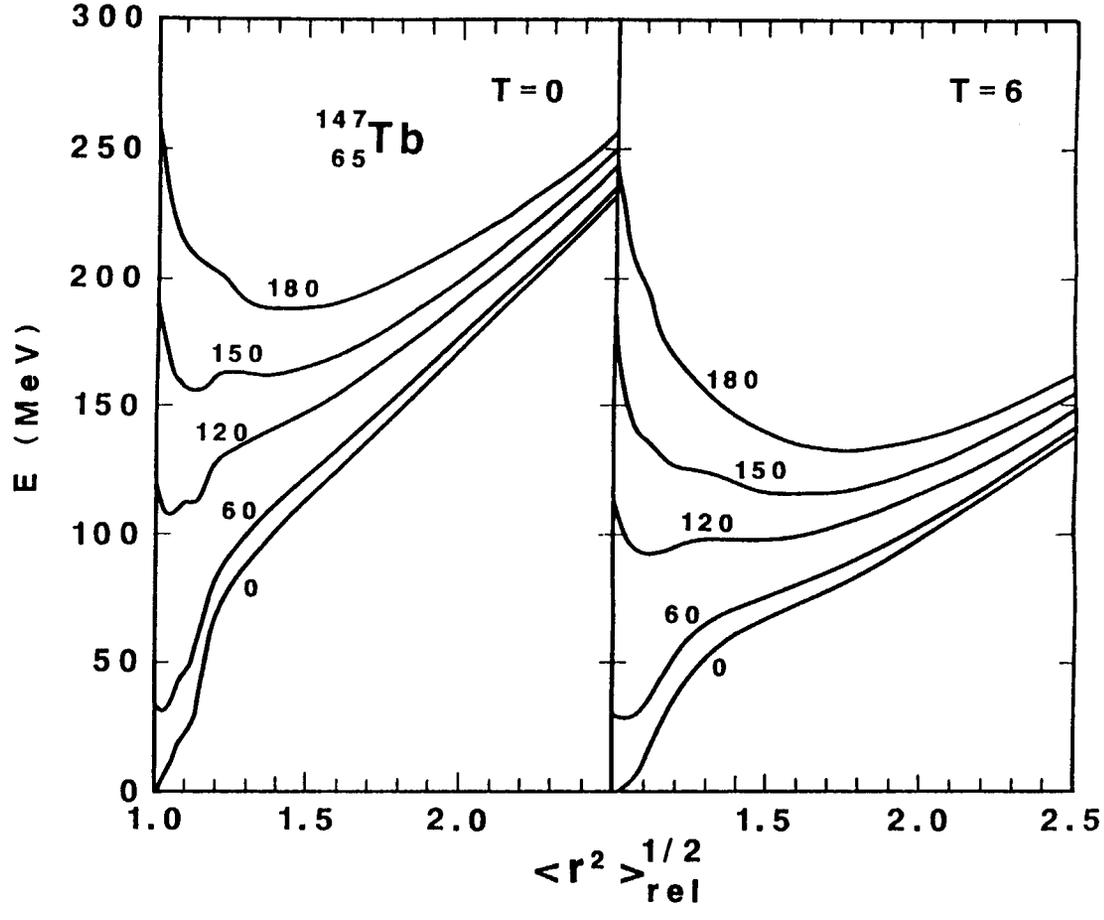

Figure 6

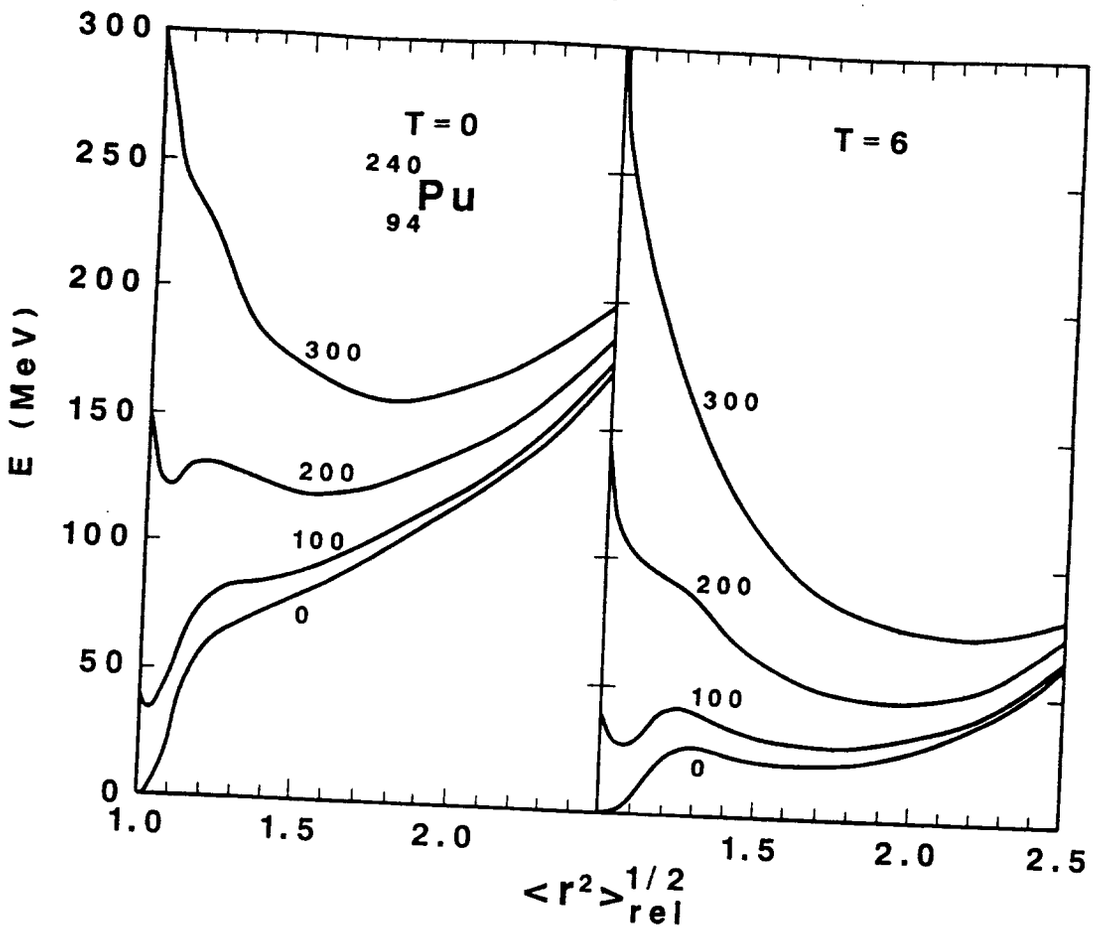

Figure 7

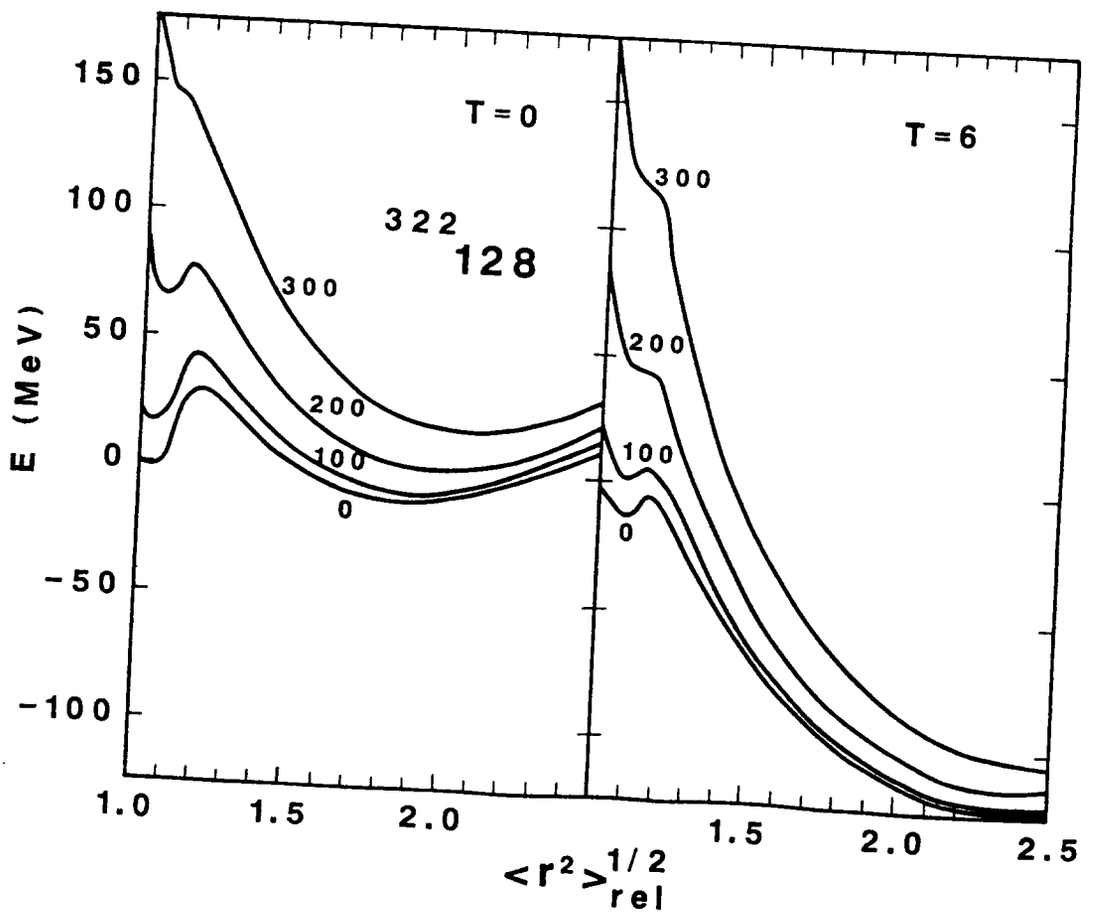

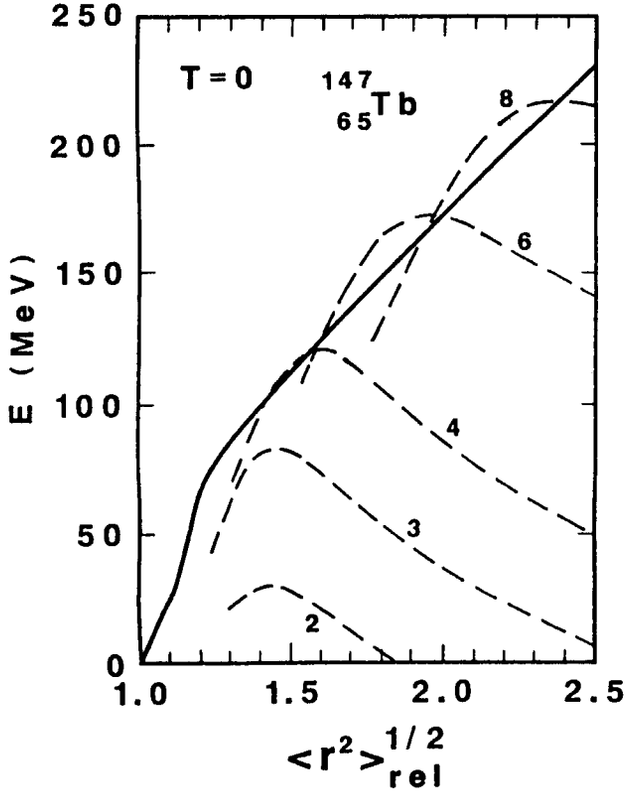

Figure 8a

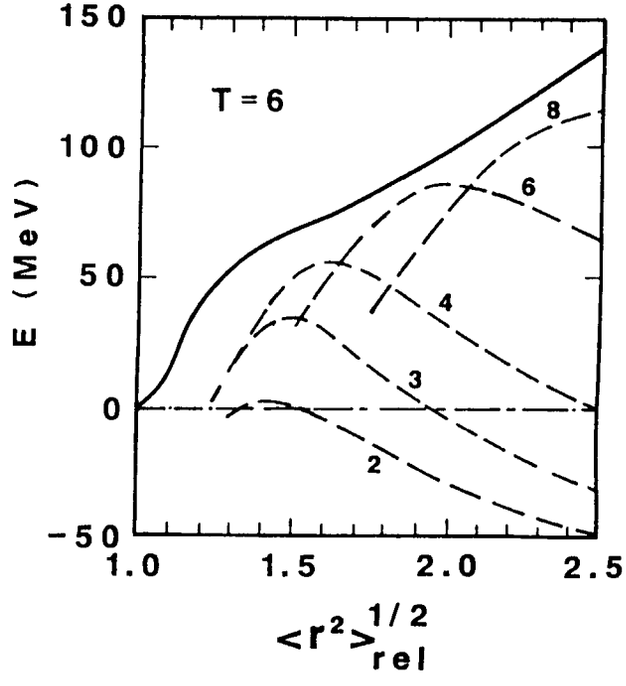

Figure 8b

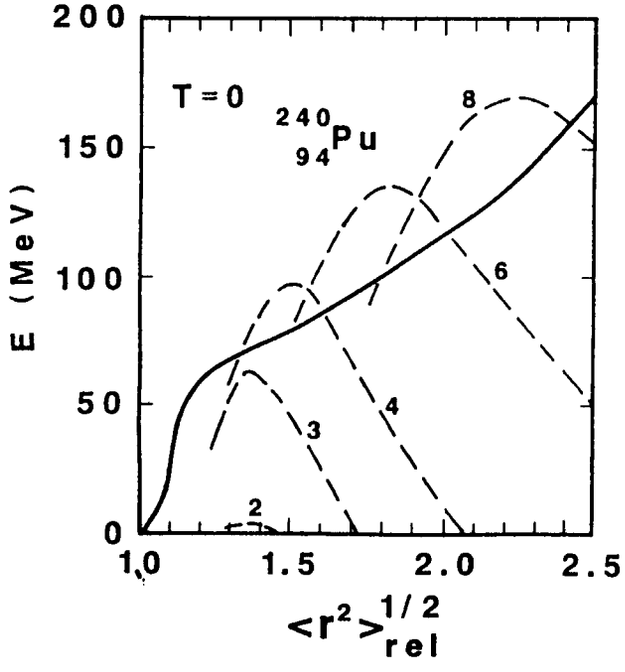

Figure 9a

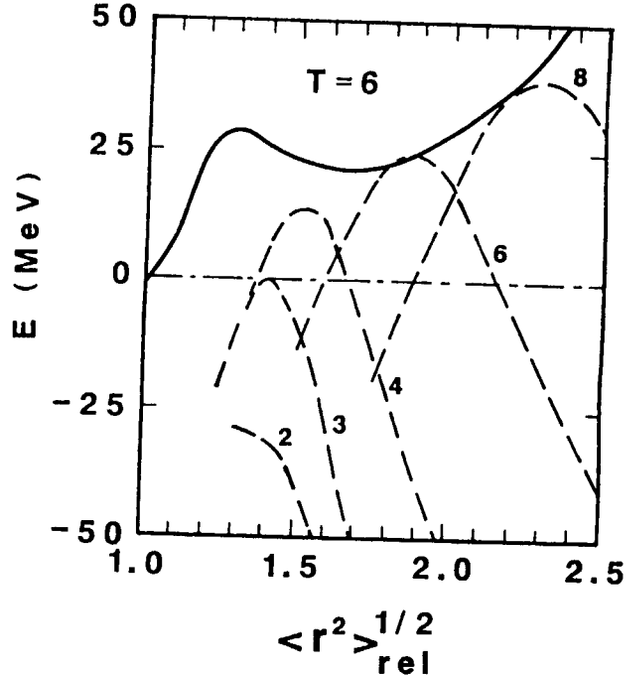

Figure 9b

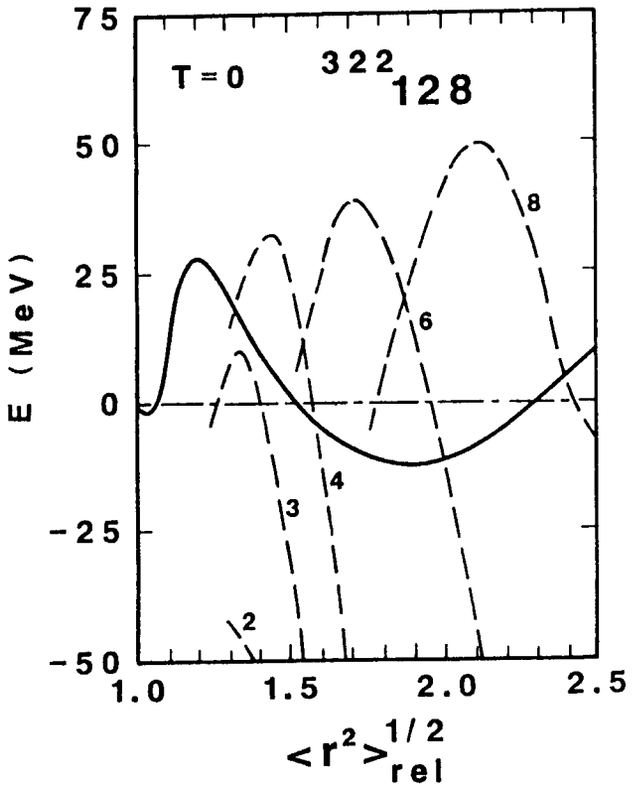

Figure 10a

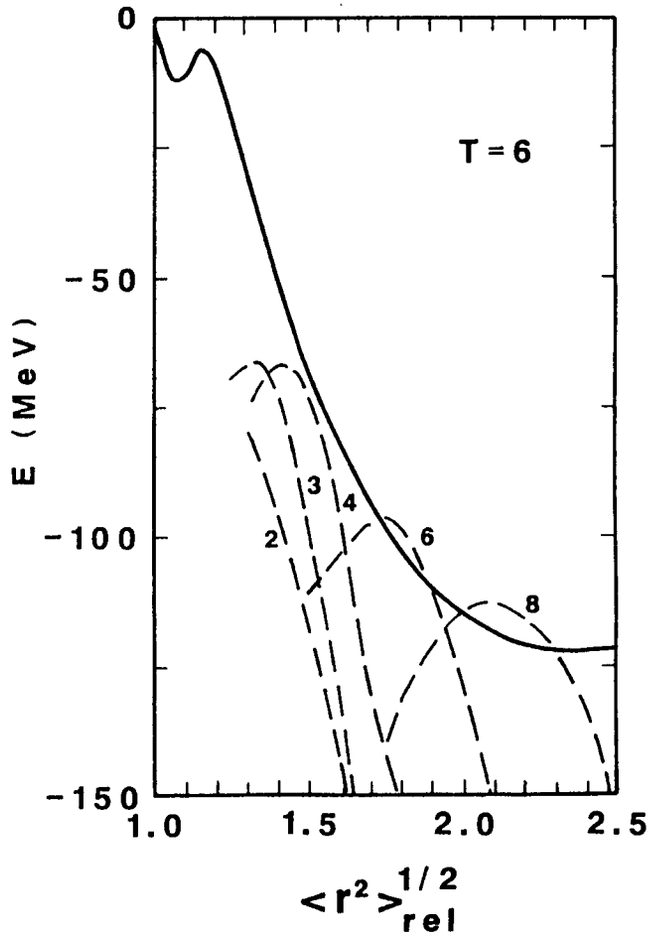

Figure 10b